Supplemental Material

An Integrated Microcircuit Model of Attentional Processing in the Neocortex

Salva Ardid, Xiao-Jing Wang, Albert Compte

This PDF file includes:

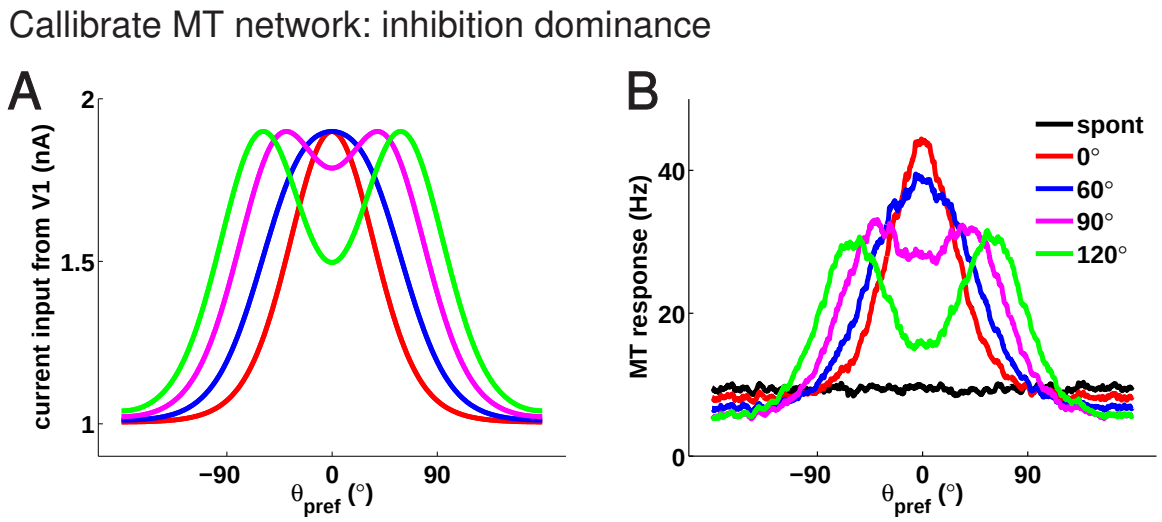

Supplemental Figure 1: The MT network model is calibrated by the constraint that the model MT neurons reproduce the responses of MT cells to transparent motion stimuli with a range of separation angle between the two motion components (Treue et al. 2000).(A) Input currents into the MT network (x-axis) for superimposed motion stimuli of various angle separations (color legend on panel (B). See Materials and Methods for details about the stimuli parameters). (B) Responses of MT neurons in the model, quantitatively very similar to the physiological data in (Treue et al. 2000). Note that the peak response is smaller for transparent motion than for single motion, and is gradually decreased with increasing separation of the two motion components. This is in contrast with the constant peak currents entering the MT network for all the stimuli (left). This phenomenon is due to synaptic suppression by MT interneurons that are driven by both bottom-up inputs (feedforward inhibition) and intrinsic MT excitatory cells (feedback inhibition). This normalization mechanism has therefore elements of previous normalization models of visual cortex (Carandini et al. 1997; Simoncelli and Heeger 1998; Rust et al. 2006).

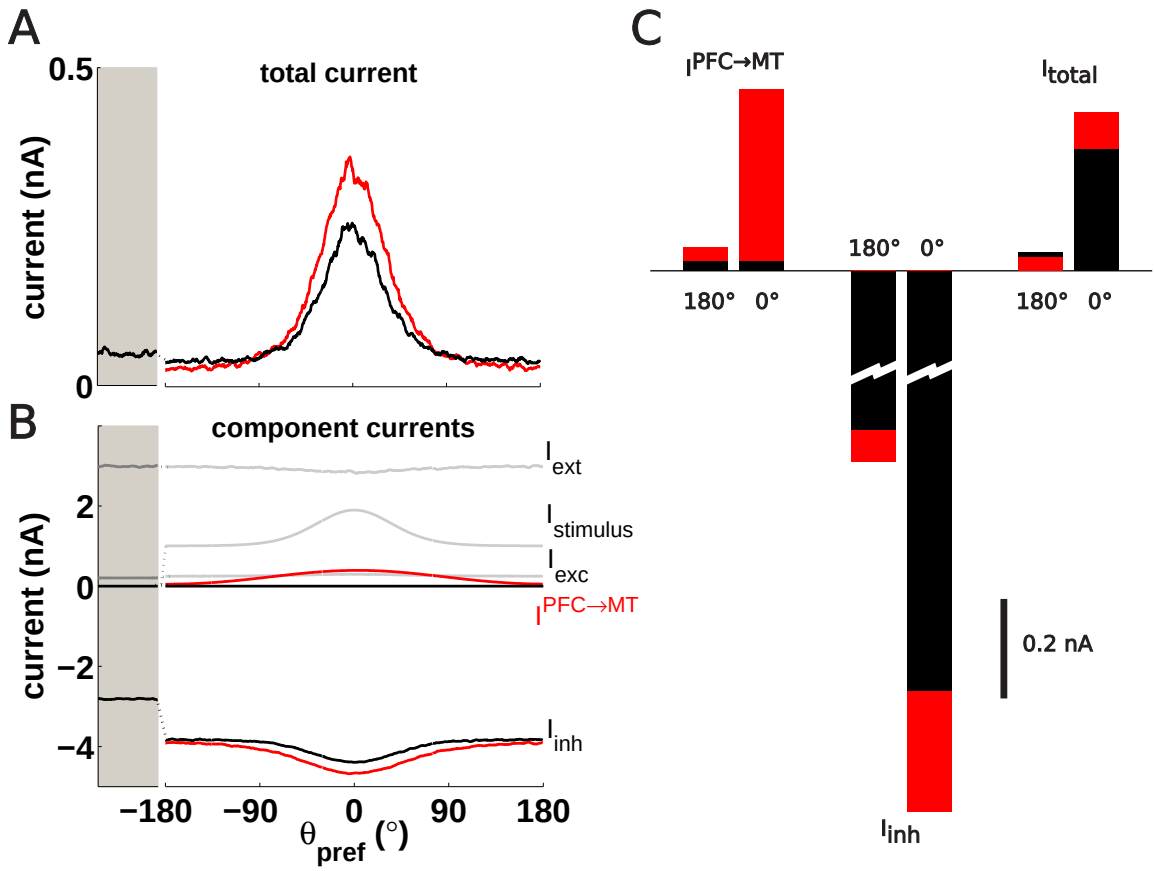

Supplemental Figure 2: Inhibitory-surround selective enhancement of population responses by attention emerges from selective top-down excitation and unspecific local-circuit inhibition. (A) Total current entering pyramidal neurons (labeled by θ_{pref} in x-axis) in the baseline (grayed area to the left), non-attended 0^{o} stimulus (black) and attention to 0^{o} stimulus (red) conditions. (B) Breakdown of incoming currents into the network model neurons in the same conditions as in (A). Currents that did not show significant variations between attended and non-attended conditions are plotted in gray (I_{exc}: recurrent excitation from network neurons; I_{ext}: external non-specific Poisson inputs; I_{stimulus}: feedforward excitation upon stimulus presentation). (C) Detail of the current balancing between contributions that did show attentional modulation ($I^{\text{PFC}\rightarrow\text{MT}}$: top-down excitatory input; I_{inh}: inhibition). For each current, the left bar corresponds to inputs into the neuron labeled 180^{o} (attention at non-preferred) and the right bar to inputs into the neuron labeled 0^{o} (attention at preferred).

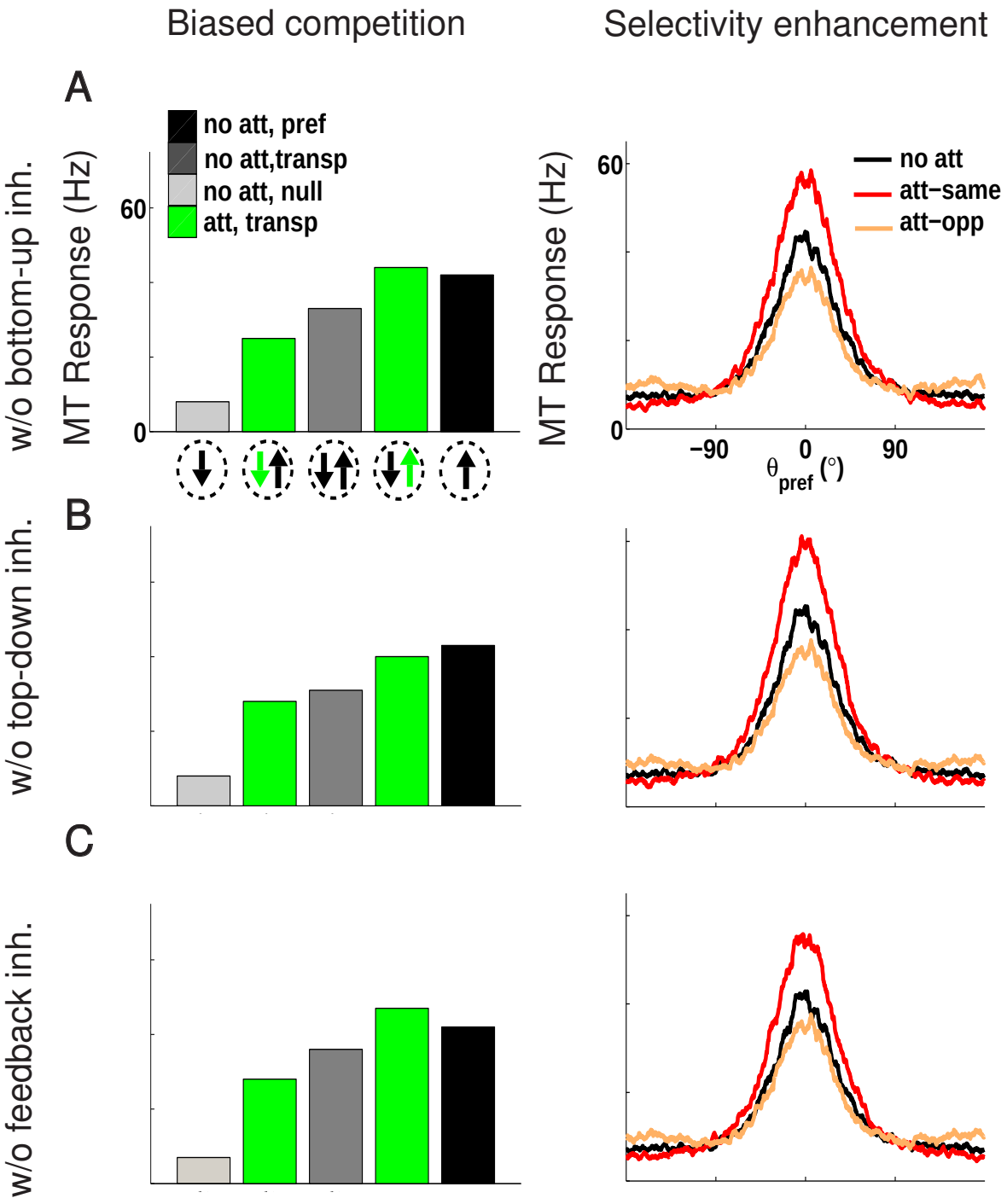

Supplemental Figure 3: (figure caption in following page)

Supplemental Figure 3: Parametric changes of the top-down input in the full model simulation revealed how selectivity enhancement (C) and multiplicative scaling (D) depended on the strengths of the PFC-to-MT conductance efficacies onto MT e-cells ($g_E^{PFC\to MT}$) and MT i-cells ($g_I^{PFC\to MT}$). To quantify selectivity enhancement of population activity and multiplicative scaling of tuning curves we computed two indices (modulation ratio MR and multiplicative index MI), schematically indicated in panels (A) and (B), respectively. For each of these quantities, we then plotted their values at the peak and tail of the corresponding curve against each other (panel (C) for MR, panel (D) for MI). Selectivity enhancement and multiplicative scaling with a 25% (50%) tolerance occur in the dark (light) gray shaded areas of each graph. Simulations for the cases of $\pm 25\%$ and $\pm 50\%$ change in $g_E^{PFC\to MT}$ and $g_I^{PFC\to MT}$ around their control values were run (i.e. 25 different parameter sets). For each set of parameters, three simulations were run: no-attention, attention-on-stimulus and attention-away-from-stimulus. Each of these conditions was repeated 10 times with different initializations of the random number generator. Data points in dark blue are obtained from the results of all corresponding pairs of simulations sharing the same parameters (i.e. attention vs. no-attention in (C), and attention-on vs. attention-off stimulus in (D)). In (D), the light blue data points correspond to the case of hypothetical additive responses. These MI values were obtained ad-hoc following one of two possible strategies: MI_{low} was not measured from simulation responses but computed using $r_{att-pref}^{low} = r_{att-null}^{low} + r_{att-pref}^{high} - r_{att-null}^{high}$, or MI_{high} was evaluated with $r_{att-pref}^{high} = r_{att-null}^{high} + r_{att-pref}^{low} - r_{att-null}^{low}$. Red data points correspond to simulations with the control parameters. Notice that for strong $g_E^{PFC\to MT}$ multiplicative scaling is progressively degraded, consistent with the proposed mechanism, as the power-law in input-output relationships applies only for sufficiently low rates (Hansel and van Vreeswijk 2002; Murphy and Miller 2003). See Mathematical analysis of the multiplicative gain modulation in supplemental Methods and supplemental Fig. 5 for details.

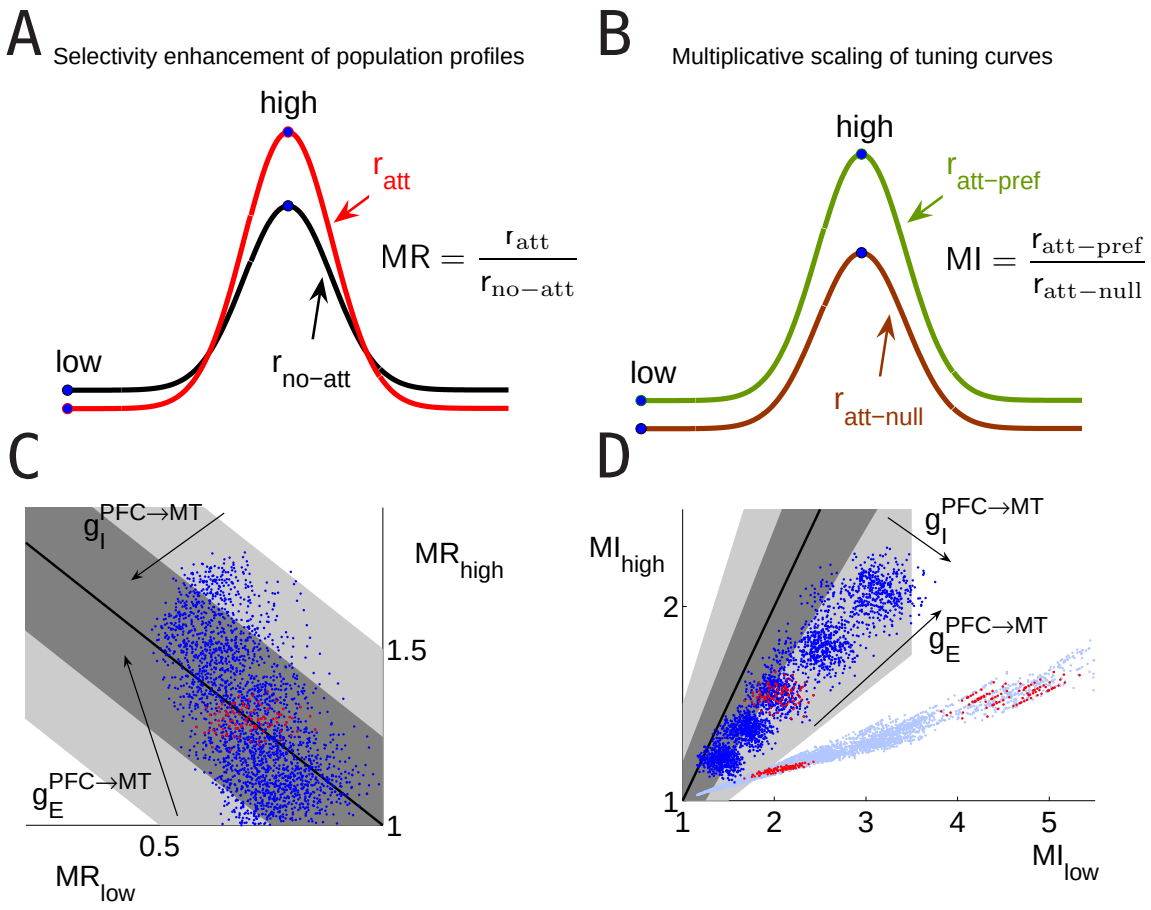

Supplemental Figure 4: Both extrinsic and recurrent inhibition in MT are required in our model simulations to obtain the biased competition and selectivity enhancement of population activity. Figure 6C and Figure 6D show that either competition or selectivity enhancement is compromised through a conjoint reduction of local excitatory drive to interneurons and either bottom-up feedforward inhibition or top-down feedforward inhibition, respectively. The conjoint inactivation is necessary, since an isolated blockade of bottom-up input (A), top-down input (B) or intrinsic excitatory drive (C), for MT interneurons does not abolish the competition in response to transparent motion stimuli, the biasing effect of attention or the selectivity enhancement of population activity. Parameter modifications were $I_0^E = 0.15$ nA, and $I_0^I = 0$ in panel (A); $G_{EE}^{PFC\rightarrow MT} = 0.098$ nS, and $G_{EI}^{PFC\rightarrow MT} = 0$ in panel (B); and $G_{EE}^{PFC\rightarrow MT} = 0.134$ nS, $I_0^E = 0.9$ nA, $I_0^I = 0.18$ nA, $G_{EI,AMPA}^{MT} = 0$, $G_{EI,NMDA}^{MT} = 0$, and $g_{ext,I} = 7.13$ nS in panel (C).

Mathematical analysis of the multiplicative gain modulation

In our model, the tuning curve of a neuron is multiplicatively scaled by attention from the unattended tuning curve (Figure 3 B), and we have argued that this multiplicative scaling is related with a power-law relationship between the firing rate and the total external input current (the sum of bottom-up and top-down inputs) in our MT excitatory cells (Figure 3 C). We have pointed out that these results support the scenario described by Hansel and van Vreeswijk (2002) and by Murphy and Miller (2003), namely a power-law input-output relationship that transforms additive inputs into multiplicative outputs. However, two main differences exist between our model and models used in those scenarios. The first difference is that we have built network models rather than single neuron models, and then, it could occur that recurrent inputs participate somehow in our multiplicative scaling. And the second difference is that both external inputs, the top-down and also the bottom-up, impact on the two kinds of cells in the MT network, the pyramidal neurons and the interneurons. Therefore, both feedforward and top-down inhibition are likely to be additionally involved in a way not accounted for previously (Hansel and van Vreeswijk 2002; Murphy and Miller 2003). To elucidate if, even with this additional complexity in our model, multiplicative scaling still relies on the power-law input-output relationship, we used a phenomenological mathematical analysis similar to the one by Murphy and Miller (2003).

The power-law input-output relationship between rate R and inputs I_S (bottom-up sensory input) and I_A (top-down attentional input) can be mathematically expressed as

$$R = a(I_S + I_A + c)^b \tag{1}$$

where a, b, and c are fitting parameters. Parameters a and b are determined by neuronal properties and the fluctuations in task-independent synaptic input, whereas parameter c is task dependent as it reflects the contribution of non-specific inhibition in the local circuit. Notice, however, that because the inhibitory input to excitatory neurons is non-specific, c reflects the mean activity of the inhibitory population and can take different values under attentional and non-attentional conditions, but does not depend on the attended feature θ_A.

Let us define $x = I_S + c$, i.e. the total input current in the non-attentional condition ($I_A = 0$).

Now, Eq. (1) can be rewritten for the non-attentional condition as

$$R_0 = ax^b \tag{2}$$

We fit with this equation the simulation data for the non-attentional condition (Figure 3 A), and this gives the factor for the power-law input-output relationship $a \simeq 1.1$ Hz/nA^b, and its exponent $b \simeq 4.0$.

Now, we consider the two relevant attentional conditions: when attention is directed to the neuron's preferred direction of motion (*att pref*) and when attention is directed to the null direction (*att null*). As we showed in Figure 3 C we have constrained the fit of these attentional conditions in two ways, on the one hand, we permitted only additive changes in current to pass from the non-attentional condition to the attentional condition. On the other hand, we fitted the two attentional conditions with the same parameters. Then, as a and b have already been determined from the fit of the non-attentional data, in the attentional conditions the only free parameter is c and it has to be exactly the same for both of them.

We define the input changes coming from attention as $\Delta x = I_A + \Delta c$. We expect that Δx is positive when attention is directed to the neuron's preferred direction, thanks to the top-down input (I_A), but negative when attention is directed to the null direction, effect that comes from the top-down inhibition included in Δc. Indeed, the values we have found are $I_A(\theta_{\text{pref}}) \simeq 0.35$ nA, $I_A(\theta_{\text{null}}) \simeq 0.04$ nA and $\Delta c = c_{\text{at}} - c_{\text{noat}} \simeq 0.42 - 0.59 = -0.17$ nA. Then, for the attentional condition Eq. (1) can be rewritten as

$$R = a(x + \Delta x)^b \tag{3}$$

Assuming a small bias ($|\frac{\Delta x}{x}| \ll 1$), we can approximate Eq. (3) to first order as

$$R \simeq ax^b + abx^{b-1}\Delta x \tag{4}$$

This assumption is justified in our model, as we have $|\frac{\Delta x}{x}| \lesssim 0.1$.

From Eq. (2) we have $x = (\frac{R_0}{a})^{1/b}$, so that Eq. (4) can be rewritten in terms of R_0 as

$$R \simeq R_0 \left[1 + \left(\frac{a}{R_0}\right)^{1/b} b\Delta x\right] \tag{5}$$

Given that R_0 is well fitted by a Gaussian function plus a constant term $r_0 + r_1 \exp[-(\theta_{\text{pref}} - \theta_S)^2/(2\sigma^2)]$ with $r_0 = 7.7$ Hz, $r_1 = 34.0$ Hz, and $\sigma = 30^\circ$ (from the tuning curve shape in Figure

3 A), the multiplicative scaling in any of the attentional conditions is reasonably approximated by

$$\frac{R}{R_0} \simeq 1 + \left[\frac{a}{r_0 + r_1 \exp\left(-\frac{(\theta_{\text{pref}} - \theta_S)^2}{2\sigma^2} \right)} \right]^{1/b} b\Delta x \tag{6}$$

In the supplemental Fig. 5 we plot the two sides of the multiplicative scaling equation (6). The left hand side is calculated numerically from the simulation data, and the right hand side is obtained from the analytical approximation in Eq. (6). Supplemental Fig. 5 shows the multiplicative scaling both when attention is located on the neuron's preference and when attention is focused on its null feature.

Notice that according to the FSGP this multiplicative scaling should correspond to a specific modulation ratio and that it must show no dependence on θ_S. Instead, Figure 5 shows a slight dependence with θ_S. This deviation from a perfect multiplicative scaling, as it has been pointed out before (Hansel and van Vreeswijk 2002; Murphy and Miller 2003), is due to the power-law shape of the input-output relationship. Although it can generate a reasonably good multiplicative scaling when its exponent is high enough, it is still not able to generate a perfect multiplication. Strictly, only the exponential function can generate exact multiplicative scaling with an additive input ($e^{x+y} = e^x e^y$). However, our observed deviations are around 5% of the multiplicative scaling mean value. This deviation is negligible when we look at the multiplicatively scaled tuning curves of Figure 3 B.

This is also the reason for deviations from multiplicative scaling in supplemental Fig. 3 D. The reason that the deviations in supplemental Fig. 3 D are higher is because the multiplicative factor is computed there between the two attentional conditions, not between attentional and non-attentional conditions as we do here. However, even for this worst possible case, the scaling is much more multiplicative than additive, as shown in supplemental Fig. 3 D.

With respect to deviations between simulation data and the analytical approximation in supplemental Figure 5, these come from considering the approximation just to first order. It can be easily shown that the second order term in the Taylor's serie is positive for the two attentional cases. Considering it, the analytical approximation of the modulaton ratio would be even much closer to the simulation data (data not shown).

We therefore conclude that the power-law input-output relationship in our model neurons

can account for the multiplicative gain modulation of neural tuning curves in all conditions of the task, provided we carefully account in addition for changes in the inhibitory drive between non-attentional and attentional conditions. The change in top-down inhibition explains the shift between curves in Figure 3 C: when we plot R versus $I_S + I_A$ there is still an additive element Δc differing between non-attentional and attentional conditions. Plotting R versus $I_S + I_A + c$ instead yields the same power-law curve for all three conditions, underscoring the fact that multiplicative responses emerge from additive inputs through the shape of the f-I curve.

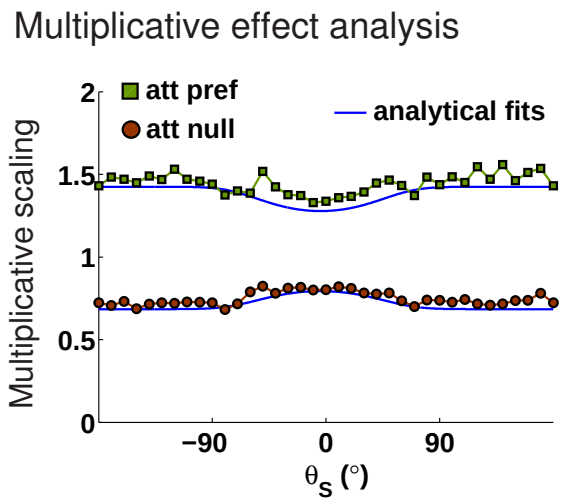

Supplemental Figure 5: Multiplicative scaling dependence on the stimulus location. Multiplicative scaling versus stimulus location for attention to preferred direction ('att pref', green squares) and attention to null direction ('att null', red circles). Simulation data results are compared with the analytical approximation, Eq. (6) in supplemental Methods (blue curves).